Effect of Ca²⁺ binding on the profile structure of the sarcoplasmic reticulum membrane using time-resolved x-ray diffraction

Laura J. DeLong, and J. Kent Blasie

Department of Chemistry, University of Pennsylvania, Philadelphia, Pennsylvania 19104 USA

ABSTRACT   A number of studies have indicated that Ca^{2+}-ATPase, the integral membrane protein of the sarcoplasmic reticulum (SR) membrane, undergoes some structural change upon Ca^{2+} binding to its high affinity binding sites (i.e., upon conversion of the E_1 to the Ca_xE_1 form of the enzyme). We have used x-ray diffraction to study the changes in the electron density profile of the SR membrane upon high-affinity Ca^{2+} binding to the enzyme in the absence of enzyme phosphorylation. The photolabile Ca^{2+} chelator DM-nitrophen was used to rapidly release Ca^{2+} into the extravesicular spaces throughout an oriented SR membrane multilayer and thereby synchronously in the vicinity of the high affinity binding sites of each enzyme molecule in the multilayer. A critical control was developed to exclude possible artifacts arising from heating and non-Ca^{2+} photolysis products in the membrane multilayer specimens upon photolysis of the DM-nitrophen. Upon photolysis, changes in the membrane electron density profile arising from high-affinity Ca^{2+} binding to the enzyme are found to be localized to three *different* regions within the profile. These changes can be attributed to the added electron density of the Ca^{2+} bound at three discrete sites centered at 5, ~30, and ~67 Å in the membrane profile, but they also require decreased electron density within the cylindrically averaged profile structure of the Ca^{2+}-ATPase immediately adjacent (<15 Å) to these sites. The locations of these three Ca^{2+} binding sites in the SR membrane profile span most of the membrane profile in the *absence* of enzyme phosphorylation, in agreement with the locations of lanthanide (Tb^{3+} and La^{3+}) binding sites in the membrane profile determined independently by using resonance x-ray diffraction.

INTRODUCTION

The sarcoplasmic reticulum (SR)[1] membrane plays a primary role in the regulation of intracellular Ca^{2+} levels involved in muscle contraction and relaxation. During relaxation, the SR integral membrane protein, Ca^{2+}-ATPase, uses ATP to actively transport Ca^{2+} from the cytoplasm, across the SR membrane, and into the sarcotubular system via a reversible, cyclic mechanism involving many steps (1).

The initial step in the forward reaction of the Ca^{2+} transport cycle of the SR Ca^{2+}-ATPase is thought to involve the binding of two Ca^{2+} ions to the high affinity binding sites on the enzyme accessible from the cytoplasmic side of the membrane (2). Previous studies have indicated that the Ca^{2+} binding kinetics are at least biphasic and that some conformational change in the enzyme may occur during Ca^{2+} binding (2–4). Obtaining structural information on the location of these Ca^{2+} binding sites on the Ca^{2+}-ATPase and the nature of the conformational change in the enzyme upon Ca^{2+} binding within a functional SR membrane should be important for developing a better understanding of the mechanism of active Ca^{2+} transport across the SR membrane.

"Large-scale" (i.e., long-range) structural changes in the Ca^{2+}-ATPase occurring during specific steps in the Ca^{2+} transport cycle have been directly investigated via time-resolved x-ray diffraction from partially dehydrated, oriented SR membrane multilayers (5–9). Such time-resolved experiments have used the flash-photolysis of the ultraviolet (UV)-sensitive molecule caged-ATP (and caged-ADP as an essential control) to initiate enzyme phosphorylation rapidly and synchronously to examine changes in the profile structure of the Ca^{2+}-ATPase within the SR membrane upon enzyme phosphorylation (i.e., upon conversion from the Ca_xE_1 to the $Ca_xE_1 \sim P$ form of the enzyme) (5). Flash-photolysis of such caged compounds provides a unique means of introducing reactive molecules into a partially dehydrated membrane multilayer specimen while preserving the orientation and ordering of the membranes in the multilayer.

We have previously studied the Ca^{2+} binding kinetics for the initial E_1 to Ca_xE_1 step employing the flash-photolysis of the caged-calcium molecule DM-nitrophen to rapidly initiate the Ca^{2+} binding reaction in fully functional, vesicular dispersions of isolated SR (4). These kinetic studies provide the basis for the structural studies described in this paper.

Changes in the meridional x-ray diffraction from partially dehydrated, oriented multilayers of isolated SR membranes upon high-affinity Ca^{2+} binding to the Ca^{2+}-ATPase were investigated to ~27-Å resolution. Flash-photolysis of the UV-sensitive calcium chelator, DM-nitrophen, was used to synchronously release Ca^{2+} throughout the extravesicular water spaces within the oriented membrane multilayer specimens. Because the multilayer profile structure can evolve slowly with time due to variation in its hydration state, it was necessary to "time resolve" even this experiment by collecting the diffraction in a series of relatively short time frames prior to and following flash-photolysis to establish that the multilayer profile structure was indeed stable both before and after the photolysis of the caged-calcium. Only for multilayer specimens exhibiting such stability could the small differences between the series of time-frames

---

[1] *Abbreviation used in this paper:* SR, sarcoplasmic reticulum.

before photolysis versus the series of time-frames after photolysis be attributed exclusively to the flash-photolysis of the DM-nitrophen in the multilayer specimen. Furthermore, a critical control experiment was used to establish that such differences were due to the binding of the photolytically released Ca^{2+} ions to the enzyme and not to specimen heating or non-Ca^{2+} photolysis products. As a result, these data were unambiguously analyzed to directly provide the electron density profile for the isolated SR membrane prior to and following the binding of Ca^{2+} ions to the Ca^{2+}-ATPase. Differences in the SR membrane electron density profile upon high-affinity Ca^{2+} binding to the enzyme, in the absence of enzyme phosphorylation, were found to be a result of Ca^{2+} binding at three discrete sites distributed across most of the membrane profile and conformational changes in the enzyme localized to within 15 Å of these sites.

MATERIALS AND METHODS

Specimen preparation

Oriented multilayers of collapsed, unilamellar vesicles were prepared by the centrifugation of a purified SR vesicular dispersion onto an aluminum foil substrate followed by controlled partial dehydration as described previously (8). The dispersions contained 1.35–1.5 mg Ca^{2+}-ATPase, 22 mM Trizma-maleate (Sigma Chemical Co., St. Louis, MO), 85 mM KCl, 8.5 mM $MgCl_2$, 7.5 mM EGTA (Sigma Chemical Co.), 15 mM DM-nitrophen (Calbiochem, San Diego, CA), pH 7.0.

DM-nitrophen is a calcium-selective, UV-sensitive calcium cage molecule that has dramatically different affinities for Ca^{2+} before (5 nM) and after (3 mM) UV-photolysis (10). It was essential to determine the concentration of residual Ca^{2+}, $[Ca_{residual}^{2+}]$, present in a particular SR vesicular dispersion ultimately to produce oriented multilayer specimens for both control and experimental trials before photolysis that possessed "Ca^{2+}-free" enzyme (e.g., $[Ca^{2+}]_{ATPase}/[Ca^{2+}$-ATPase] < 10^{-1}, where $[Ca^{2+}]_{ATPase}$ denotes Ca^{2+} bound to the enzyme), and to determine that after photolysis, the enzyme in the control trials continued to remain "Ca^{2+} free." The $Ca_{residual}^{2+}$ concentration for each preparation was determined spectrophotometrically using a time-sharing, dual-wavelength spectrophotometer, as described elsewhere (11), that monitored changes in the absorption spectrum of the metallochromic indicator Arsenazo III (Sigma Chemical Co., St Louis, MO) upon titration of Ca^{2+} with EGTA. The $Ca_{residual}^{2+}/Ca^{2+}$-ATPase mole ratio was thereby determined to be 1–1.5:1. All the oriented multilayer specimens for the x-ray diffraction experiments therefore included enough EGTA estimated to chelate this $Ca_{residual}^{2+}$ (see below). The experimental trials included an additional 15-mM $CaCl_2$, which we estimated (see below) would give the experimentals a 15-mM DM-nitrophen:calcium complex along with a <7.5 mM EGTA:$Ca_{residual}^{2+}$ complex whereas the controls were estimated to have a <7.5 mM DM-nitrophen:$Ca_{residual}^{2+}$ complex before photolysis. Upon photolysis, the experimental trials were then estimated to contain a $[Ca^{2+}]_{ATPase}/$ $[Ca^{2+}$-ATPase] molar ratio of 2–3 (the $[Ca^{2+}$-ATPase] being ~5 mM in the oriented multilayer specimens) whereas the $Ca_{residual}^{2+}$ released in the control trials was estimated to bind solely to the EGTA, which has a K_d intermediate (~10^{-7} M [12, 13]) between that of the unphotolyzed DM-nitrophen (~5 nM) and that of the high affinity binding sites on the Ca^{2+}-ATPase (~10^{-6} M [2]) under our conditions. The overall experiment was thus designed such that upon photolysis, the experimental trials would release Ca^{2+} that would be accessible only to the enzyme's high affinity binding sites whereas the control trials would not, all other conditions being equivalent (i.e., UV energy dissipated as

heat, non-Ca^{2+} photolysis products, etc.). (Note: Given the K_d's and concentrations of the various components provided above, a simple calculation [treating the several equilibria involved independently, giving the lower K_d components higher priorities] provides an estimate of the maximum $[Ca^{2+}]$ available to the Ca^{2+}-ATPase in the experimental trials of 42–63 μM before photolysis and a maximum $[Ca^{2+}]$ available to the enzyme in the control trials of ≤6 μM before photolysis; thus, for a $[Ca^{2+}$-ATPase] of 5 mM in the oriented multilayers, the $[Ca^{2+}]_{ATPase}/[Ca^{2+}$-ATPase] ratio was anticipated to be ≤10^{-2} before photolysis for both the experimental and control trials. After photolysis, the maximum $[Ca^{2+}]$ available to the enzyme in the control trials was estimated to be 33–54 μM again, providing a $[Ca^{2+}]_{ATPase}/$ $[Ca^{2+}$-ATPase] ratio of ≤10^{-2}. Hence, we anticipated that <1 Ca^{2+} ion per 100 Ca^{2+}-ATPase molecules would be available to bind to the enzyme's high affinity binding sites of $K_d \cong 10^{-6}$ M in both the experimental and control trials before photolysis and also in the control trials after photolysis. Conversely, we expected there to be only two to three Ca^{2+} ions available to bind per enzyme to its high affinity binding sites in the experimental trials after photolysis. Therefore, the differences in the profile structure of the SR membrane detected upon photolysis in the experimental trials, but not in the control trials, were expected to arise at least predominantly from the binding of Ca^{2+} ions to the enzyme's high affinity binding sites, since the lower affinity Ca^{2+} binding sites in the SR membrane (e.g., phospholipid headgroups) have K_d's >10^{-3} M. These initial estimates of $[Ca^{2+}]_{ATPase}/[Ca^{2+}$-ATPase] for the control and experimental trials before and after photolysis upon which these experiments were based have subsequently been further analyzed, taking into full account the interactions between the multiple equilibria involved (see Discussion).

The wet ultracentrifugal pellets of isolated SR vesicles on aluminum foil were mounted on cylindrically curved glass slides and were partially dehydrated slowly over a saturated salt solution for 12–19 h (KCl, 88%) at 7 ± 0.5°C to produce the oriented multilayer specimens. This temperature was selected to be consistent with earlier work from our laboratory under similar conditions (14, 15). The specimens were then placed in a sealed canister with appropriate aluminum foil and Mylar windows (for x-ray and UV, respectively) and maintained at a constant relative humidity of 95 ± 0.4% at the same temperature via a humidity generator for the duration of the diffraction experiment. The humidity generator used a monitor (model Hygro-M2; General Eastern Instruments, Watertown, MA), measuring the relative humidity via an optical condensation dewpoint hygrometer (model 1111H; General Eastern Instruments) for a mixture of wet and dry helium gas controlled via a process controller (model 2101; Omega Engineering, Inc., Stamford, CT) with feedback from the monitor. The moist helium was pumped continuously through the multilayer specimen chamber (the chamber and the generator forming a closed loop) thereby precisely controlling the relative humidity of the SR membrane multilayer's environment.

The photolysis light was provided by a UV band-pass (passing mostly 300–350 nm) filtered (filter No. UG11; Rolyn Optics, Covina, CA), 200-W mercury arc lamp delivered to the multilayer surface from a distance of 15 mm via a liquid light guide (Oriel Optics, Stratford, CT), which thereby fully illuminated the multilayer. The photolysis time was based on our previous spectrophotometric studies with DM-nitrophen and vesicular SR dispersions, our knowledge of the photolysis times of caged-ATP within an oriented SR membrane multilayer specimen, and the quantum yield of c-ATP (0.55) (16) versus DM-nitrophen (0.18) (17), all of which indicated that 1 min would be ample time to produce the maximum mole ratio of released-Ca^{2+}/Ca^{2+}-ATPase of 2–3 in a multilayer specimen.

X-ray diffraction experiments

An Elliot GX-13 rotating anode x-ray generator (Enraf-Nonius, Bohemia, NY) and a cylindrically bent, asymmetrically cut Ge (111) monochromator crystal were used to produce an x-ray beam (CuK$_{\alpha1}$) that was line-focused at an optimal distance 1,300 mm downstream. This beam was directed for grazing (tangential) incidence to the cylindri-

cally curved multilayer surface with the line-focus parallel to the specimen cylinder axis. The specimen to detector distance was 640–650 mm and the beam height at the specimen was 4 mm, with all beam paths in helium. The meridional x-ray diffraction patterns from the oriented, SR membrane multilayer specimens were collected in consecutive 5-min time frames with a two-dimensional (2-D), position-sensitive proportional counter (Seimens Instruments, Madison, WI) interfaced to a GPXII Microvax computer system (Digital Equipment Corp., Marlboro, MA) and stored as 2-D data files.

These 2-D data files were then integrated perpendicular to the meridional axis over a strip whose width was sufficient to include the extent of the meridional diffraction in this direction due to x-ray beam height and multilayer specimen mosaic spread (layer misorientation) to produce a one-dimensional (1-D) data file $[I_t(z^*)]$ containing the meridional x-ray diffraction as the number of x-ray counts versus detector channel number over 512 channels, each channel corresponding to a particular value of the meridional reciprocal space coordinate $z^* = 2 \sin \theta / \lambda$. The resulting 1-D data files were transferred to a VAX 11/750 computer (Digital Equipment Corp.) for further analysis.

Data analysis

Initially, the 5-min time frames for the "raw" (i.e., uncorrected for meridional background scattering) meridional x-ray diffraction, $[I_t(z^*)]$, collected immediately preceding and immediately following flash-photolysis of the DM-nitrophen in the multilayer specimens were normalized to have the same total counts integrated over z^* and the difference $[I_t(z^*)_{after} - I_t(z^*)_{before} = \Delta I_t(z^*)]$ calculated to determine if there were any obvious differences in the behavior of the control versus the experimental trials. This simple arithmetic difference between two sequential time frames of such raw meridional diffraction data provided an unbiased examination of the changes occurring in the meridional diffraction upon flash-photolysis, but with poor counting statistics.

To improve the counting statistics in $\Delta I_t(z^*)$, sequential time frames collected before and after photolysis were summed to yield cumulative raw $I_t(z^*)^{sum}$ data before and after photolysis, provided that the multilayer specimens were stable before and after photolysis. The stability, or lack thereof, of the various multilayer specimens for both the control and experimental trials was determined by inspection of the differences between any pair of 5-min time frames in a sequence of consecutive time frames either before or after photolysis; any signal above counting statistics in one or more such differences either before or after photolysis resulted in rejection of all data from that particular specimen.

The meridional background scattering $[B(z^*)]$ was determined for the cumulative meridional diffraction pattern before photolysis $I_t(z^*)^{sum}_{before}$ for each stable multilayer specimen and removed by subtraction. The background scattering function $B(z^*)$ consisted of a piecewise continuous exponential function fitted to the minima in $I_t(z^*)^{sum}_{before}$ separating the three regions of constant phase in the meridional diffraction from an oriented SR membrane multilayer (see Fig. 3 A). Because the changes in the meridional diffraction upon photolysis of DM-nitrophen in the multilayer are small in comparison with the total meridional diffraction, an error in the background scattering correction for $I_t(z^*)^{sum}_{before}$ could unintentionally bias the meridional difference diffraction, $\Delta I_c(z^*)^{sum} = [I_c(z^*)^{sum}_{after} - I_c(z^*)^{sum}_{before}]$, corrected for the meridional background scattering. For this reason the background-corrected, meridional difference diffraction data $\Delta I_c(z^*)^{sum}$ were determined using a method similar to that described for the treatment of resonance x-ray diffraction data (15). The background corrected difference, $\Delta I_c(z^*)^{sum}$, was determined using the raw difference, $\Delta I_t(z^*)^{sum}$, where $\Delta I_t(z^*)^{sum} = [I_t(z^*)^{sum}_{after} - I_t(z^*)^{sum}_{before}]$, in a manner that insures that the same background scattering function $B(z^*)$ is subtracted in precisely the same way from both the $I_t(z^*)^{sum}_{before}$ and $I_t(z^*)^{sum}_{after}$; namely for

$$I_c(z^*)^{sum}_{before} = I_t(z^*)^{sum}_{before} - B(z^*),$$

then

$$I_c(z^*)^{sum}_{after} = \Delta I_t(z^*) + I_c(z^*)^{sum}_{before}.$$

A Lorentz correction (18) of z^*, which compensates for the cylindrical curvature of the multilayer specimen, was applied to the background-corrected, cumulative diffraction patterns $I_c(z^*)^{sum}$ before and after photolysis. This final correction then provided the square of the unit cell structure factor modulus $|F_{uc}(z^*)|^2$ for the multilayer unit cell electron density profile $\rho_{uc}(z)$. These background-corrected, cumulative diffraction patterns $I_c(z^*)^{sum}$ were then subjected to Fourier analysis to obtain the correct phase combination for the unit cell structure factor, $F_{uc}(z^*)$, and thereby the corresponding multilayer unit cell electron density profile, $\rho_{uc}(z)$.

RESULTS

Effect of photolysis on the meridional x-ray diffraction

Inspection of the difference $\Delta I_t(z^*)$ between the two successive 5-min time frames of the raw meridional x-ray diffraction, namely the first immediately after photolysis of the DM-nitrophen in the multilayer, $[I_t(z^*)_{after}]$, minus the last immediately before photolysis, $[I_t(z^*)_{before}]$, indicates that small changes in the raw $I_t(z^*)$ occur upon photolysis, which exceed the counting statistics and are similar among the experimental trials, and that no such changes are evidenced in the control trials. These differences $\Delta I_t(z^*)$ are shown for four experimental trials and four control trials in Fig. 1.

The cumulative difference $\Delta I_t(z^*)^{sum}$ for specimens that were stable, by the criteria described in the Materials and Methods, over a total time period (before and after photolysis) of 55–70 min are shown in Fig. 2 for two experimental and two control trials. With an improved signal-to-noise level the changes seen in Fig. 1 are much more pronounced for the two experimental trials shown in Fig. 2 whereas some smaller changes are now evident in the two control trials (with the improved signal-to-noise level), which are similar for the two control trials and distinctly different from the changes exhibited by the two experimental trials.

Fig. 3 A shows a semilog plot of the cumulative, raw meridional x-ray diffraction, $\ln [I_t(z^*)^{sum}]$, from a stable, oriented SR membrane multilayer specimen before photolysis, including its estimated meridional background scattering, $B(z^*)$. Fig. 3 B shows its corresponding difference diffraction, $\Delta I_t(z^*)^{sum}$, scaled up by a factor of 20. The changes in the meridional diffraction for this stable experimental trial upon photolysis of the DM-nitrophen in the multilayer are small (<5% of the raw meridional diffraction), but experimentally significant. The change indicated by the arrow (a) corresponds to a decrease in the first-order reflection, the arrow (b) corresponds to a slight decrease in the region of the second-order reflection, and the area (c) indicates an increase
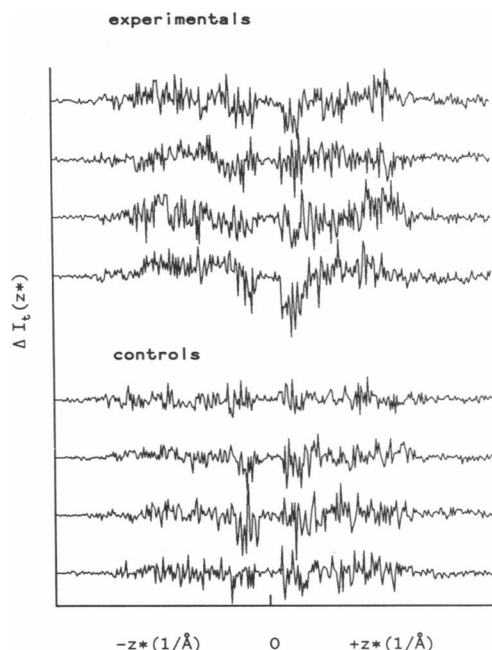
experimentals

controls

$-z*(1/Å)$ 0 $+z*(1/Å)$

FIGURE 1   The difference, $\Delta[I_t(z)^*]$, between two successive 5-min time frames of the raw meridional x-ray diffraction from oriented SR membrane multilayers, specifically for the first immediately after photolysis of the DM-nitrophen in the multilayer, $[I_t(z^*)_{after}]$, minus the last immediately before photolysis, $[I_t(z^*)_{before}]$. This difference is shown for four experimental trials, in which the photolytically released free Ca^{2+}/Ca^{2+}-ATPase molar ratio was 2–3, and four control trials, in which the photolytically released free Ca^{2+}/Ca^{2+}-ATPase molar ratio was essentially zero.

over the region of the broad third- and fourth-order reflections, the oriented multilayer possessing a relatively large amount of lattice disorder of the second kind typical of these specimens. The meridional x-ray diffraction maxima at larger values of $z^* > 0.021$ $Å^{-1}$ in Fig. 3 A exhibited only very small changes relative to those occurring for $z^* < 0.021$ $Å^{-1}$ upon photolysis for the stable experimental trials.

Derivation of the SR membrane electron density profiles

The cumulative, background scattering–corrected meridional x-ray diffraction data before and after flash-photolysis of the DM-nitrophen in the stable experimental trial specimens, namely $I_c(z^*)_{before}^{sum}$ and $I_c(z^*)_{after}^{sum}$, were analyzed independently using the Generalized Fourier Synthesis Deconvolution Method (GFSDM) (19), which assumes only a centrosymmetric profile structure for the flattened, unilamellar SR membrane vesicle contained within the multilayer unit cell and allows an unambiguous determination of the unit cell relative electron density profile containing the two apposed single membrane profiles taking into full account the nature of the multilayer lattice including periodicity and disorder.

The analysis was carried out to a spatial resolution of ~27 Å (i.e., employing data out to $(z^*)_{max} \sim 1/27$ Å) since there were no changes in the meridional diffraction maxima upon photolysis for the experimental trials evident beyond this value of z^*. Fig. 4 A shows the so-derived unit cell relative electron density profiles, $[\rho_{uc}(z)]$, for an experimental trial before and after photolysis at 27-Å resolution. The small changes in the unit cell relative electron density profile upon photolysis evident in Figure 4 A are shown in Fig. 4 B as the difference between these two electron density profiles, $[\Delta\rho_{uc}(z)]$, scaled up by a factor of 20. Use of the GFSDM analysis ensures that these so-derived changes in the unit cell relative electron density profile are unaffected by any possible changes in the multilayer lattice parameters, which did not change upon photolysis in either the experimental or control trials.

Model refinement of the SR membrane electron density profiles

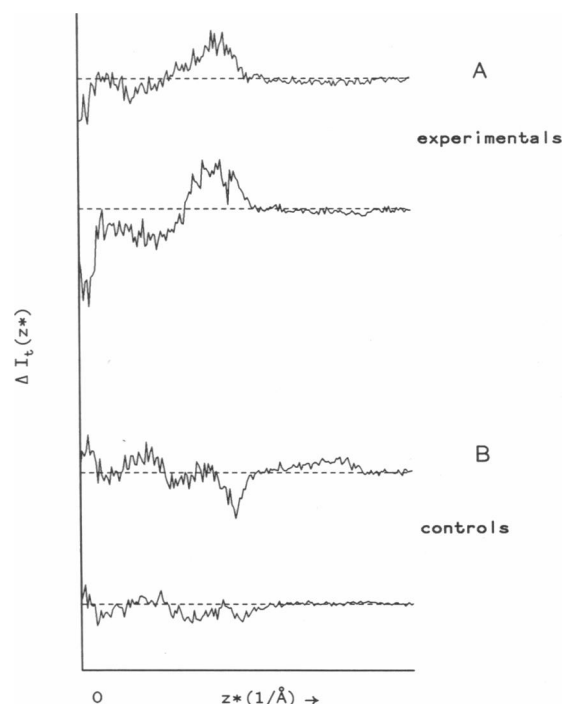To interpret the changes in the single SR membrane relative electron density profile within $[\rho_{uc}(z)]$ in terms of

FIGURE 2   Cumulative difference, $[\Delta I_t(z^*)^{sum}]$, between summed sequential 5-min time frames of the raw meridional x-ray diffraction, $[I_t(z^*)^{sum}]$, collected from oriented SR membrane multilayer specimens immediately before, $[I_t(z^*)_{before}^{sum}]$, and immediately after, $[I_t(z^*)_{after}^{sum}]$, photolysis for (A) two experimental and (B) two control specimens that were stable for a total time period of 55–70 min before and after photolysis of the DM-nitrophen in the multilayer. The criteria for multilayer stability are described in the text and the improved statistics are readily apparent. The horizontal dashed line represents the $\Delta[I_t(z^*)^{sum}] = 0$ level in each.
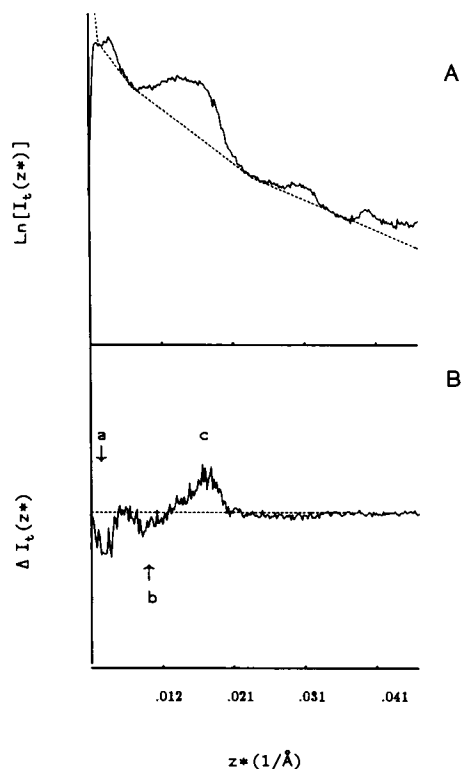
density model profile, $[\rho_{uc}^{mod}(z)]$ (*dotted line*), compared with the experimentally derived $[\rho_{uc}^{exp}(z)]$ (*solid line*) for an experimental trial specimen before photolysis. Based on our previous work (9), steps 1 and 4 contain the phospholipid polar headgroups of the inner and outer monolayers, respectively, and Ca^{2+}-ATPase protein; steps 2 and 3 contain the fatty acyl chains of the inner and outer monolayers, respectively, and Ca^{2+}-ATPase protein; and the outer three steps (5, 6, and 7) are located outside the membrane phospholipid bilayer and contain water and $\sim50\%$ of the Ca^{2+}-ATPase protein (see reference 9 for details).

A refined step-function model profile was then developed via a similar real-space refinement analysis for the changes in the unit cell electron density profile, $\Delta\rho_{uc}(z)$, upon photolysis of the DM-nitrophen in the stable experimental trial specimens, using the comparison of the corresponding continuous, difference electron density model profile, $\Delta\rho_{uc}^{mod}(z)$, and the experimental $\Delta\rho_{uc}^{exp}(z)$. In this real-space refinement analysis, we

FIGURE 3 (*A*) Semilog plot of the cumulative, raw meridional x-ray diffraction, $\ln[I_t(z^*)^{sum}]$, from a stable, oriented SR membrane multilayer specimen at $7°C$ before photolysis and the estimated meridional background scattering, $[B(z^*)]$ (*dotted line*). (*B*) The corresponding difference $\Delta[I_t(z^*)]^{sum}$ scaled up by 20×.

the molecular components of the SR membrane, a step-function model refinement analysis was performed in real space. The initial step-function model electron density profile was based on a refined step-function model profile for the SR membrane established previously for the Ca_xE_1 form of the ATPase at a higher resolution of ~15 Å (14) since the SR membrane multilayers used in this study did indeed exhibit meridional x-ray diffraction to a comparable spatial resolution. This model was Fourier transformed to provide its corresponding unit cell structure factor $F_{uc}^{mod}(z^*)$, truncated below $(z^*)_{min}$ and above $(z^*)_{max}$ to match that of the experimental meridional diffraction data, and finally inverse Fourier transformed to obtain the continuous electron density profile $\rho_{uc}^{mod}(z)$ corresponding to the step-function model. The initial step-function model was then refined by systematic variation of the amplitude of the steps while maintaining their width at a 13–16-Å spatial resolution limit until a good match between $\rho_{uc}^{mod}(z)$ and the experimental electron density profile, $\rho_{uc}^{exp}(z)$, was achieved. Such a match resulted in the normalized least-squares fit of the model unit cell structure factor modulus squared, $|F_{uc}^{mod}(z^*)|^2$, to the experimental $|F_{uc}^{exp}(z^*)|^2$ of $>0.1\%$. Fig. 5 shows the refined step-function model profile (*dashed line*) for the SR membrane along with its corresponding continuous electron
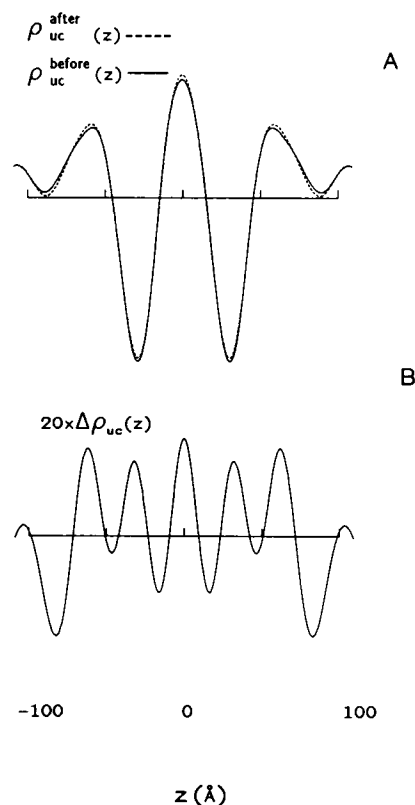
FIGURE 4 (*A*) Unit cell relative electron density profiles, $[\rho_{uc}(z)]$, for the apposed SR membrane pair at 27-Å resolution before (*solid line*) and after (*dashed line*) photolysis of the DM-nitrophen in the multilayer. These profiles were calculated via GFSDM analysis of the corresponding $I_c(z^*)_{before}^{sum}$ and $I_c(z^*)_{after}^{sum}$ corrected meridional diffraction data resulting in the phase combination $\pi, 0, \pi$ for the first three diffraction maxima. The unit cell profile dimension (or multilayer periodicity) was 218 Å. (*B*) The difference unit cell relative electron density profile $[\Delta\rho_{uc}(z)]$ scaled up by 20× for the apposed SR membrane pair calculated as $[\Delta\rho_{uc}(z)] = [\rho_{uc}^{after}(z)] - [\rho_{uc}^{before}(z)]$.

y-axis: $\rho_{uc}(z)$
legend: exp ——, model ----
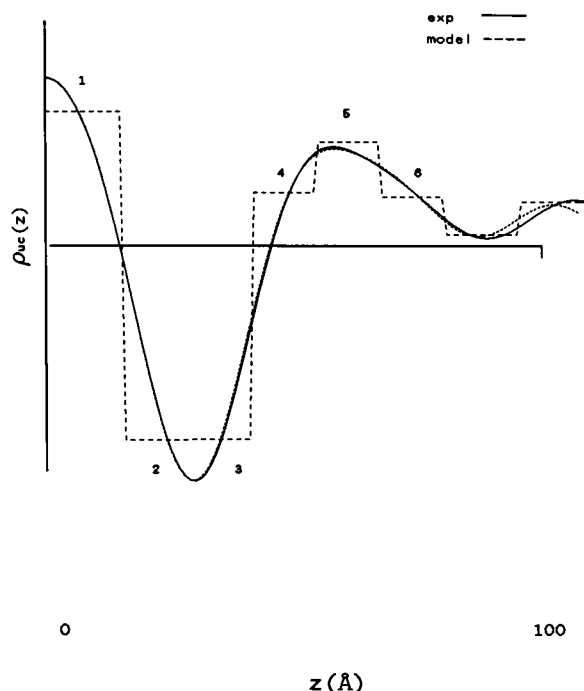x-axis: $z\,(\text{Å})$, from 0 to 100

FIGURE 5 The refined step-function model profile (*dashed line*) for the SR membrane profile using 8 resolution-limited steps per single membrane profile (or 16 steps over the unit cell profile). The corresponding continuous relative electron density profile, $[\rho_{uc}^{mod}(z)]$ is shown (*dotted line*) for comparison with the experimentally derived (via GFSDM analysis) $[\rho_{uc}^{exp}(z)]$ (*solid line*).

at a low spatial resolution of ~ 27 Å, because of the correlation with its counterpart in the apposed membrane profile within the multilayer unit cell profile over a relatively large distance across the intravesicular water space. Thus, the precisions stated for these positions are indeed ± 0.1–0.2 Å.)

DISCUSSION

We have demonstrated that significant changes occur in the meridional x-ray diffraction from an oriented multilayer of isolated SR membranes upon flash-photolysis of a DM-nitrophen:Ca^{2+} complex in the multilayer resulting in an estimated $[Ca^{2+}]_{ATPase}/[Ca^{2+}\text{-ATPase}]$ molar ratio of 1–1.5. The experimental trials exhibited small, but experimentally significant (in terms of signal to

sought a step-function model profile containing the *minimum* number of steps, whose widths were again limited to be greater than or equal to the spatial resolution limit used in modeling $\rho_{uc}(z)$, which could achieve a good match between $\Delta\rho_{uc}^{mod}(z)$ and $\Delta\rho_{uc}^{exp}(z)$. A minimum number of six steps per single membrane profile were thereby required to achieve such a match that resulted in a least-squares fit of the difference structure factor modulus squared for the model, $|\Delta F_{uc}^{mod}(z^*)|^2$, to the experimental difference structure factor modulus squared, $|\Delta F_{uc}^{exp}(z^*)|^2$ of $<2\%$, as shown in Fig. 6 *A*. Fig. 6 *B* shows this refined step-function model (*dashed line*), along with its corresponding continuous $[\Delta\rho_{uc}^{mod}(z)]$ (*dotted line*) and the experimentally derived $[\Delta\rho_{uc}^{exp}(z)]$ (*solid line*). Similar results were obtained with the other stable experimental trial specimens. The three positive steps 1, 3, and 5, are centered at 5, 29.5, and 66.5 Å for this particular sample. Analysis of other experimental trial specimens indicates that the center of these steps remain the same (to within ± 2 Å), taking into account variations in the periodicity of the multilayer lattice and the resulting variation in the extent of the intravesicular water space separating the two apposed membrane profiles within the multilayer unit cell. (It should be noted that such a real-space refinement analysis is very sensitive to the position of the center of each of the finite number of steps within a single membrane profile, even

A
y-axis: $|\Delta F_{uc}(z^*)|^2$
legend: exp ——, model ----
x-axis: $z^*\,(\text{Å})$, from 0 to z^*_{max}

B
y-axis: $\Delta\rho_{uc}(z)$
legend: exp ——, model ----
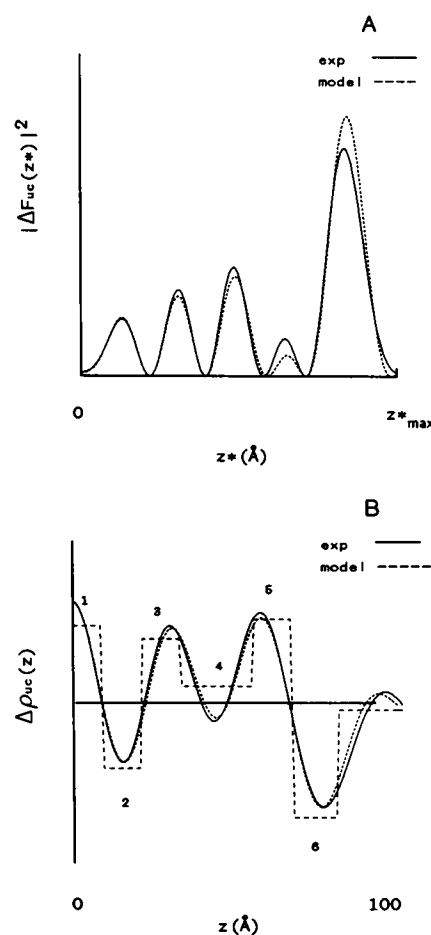x-axis: $z\,(\text{Å})$, from 0 to 100

FIGURE 6 The model (*dotted line*) unit cell structure factor modulus squared, $|\Delta F_{uc}^{mod}(z^*)|^2$, corresponding to the refined step-function model profile (shown in *B, dashed line*) for the difference electron density profile, $[\Delta\rho_{uc}^{exp}(z)]$ as compared with the latter's corresponding experimental unit cell structure factor modulus squared, $|\Delta F_{uc}^{exp}(z^*)|^2$ (*solid line*). (*B*) The refined step-function model profile (*dashed line*) for the changes in the unit cell relative electron density profile upon photolysis of the DM-nitrophen in the multilayer for the experimental trials, $[\Delta\rho_{uc}^{exp}(z)]$ (*solid line*), and, for comparison, the model's corresponding continuous profile, $[\Delta\rho_{uc}^{mod}(z)]$ (*dotted line*).

noise) and reproducible changes upon photolysis, whereas the controls generally exhibited no such changes upon photolysis resulting in an estimated $[Ca^{2+}]_{ATPase}/[Ca^{2+}\text{-ATPase}]$ of $<10^{-2}$. The "smallness" of the changes in the meridional x-ray diffraction upon photolysis in the experimental trials was not unanticipated, was therefore incorporated into the design of these experiments and is fully consistent with their structural origin (see below). The fact that these small changes are manifest in the meridional x-ray diffraction primarily for $z^* \leq 1/27$ Å (and therefore in the membrane profile at 27-Å resolution) is simply a consequence of there being two apposed single membrane profiles in the multilayer unit cell profile; any (even a small) change in the profile of one of the membrane profiles away from the intravesicular membrane surface is automatically manifest at low values of z^* through the correlation with its counterpart in the other apposed membrane profile over a relatively "large" distance across the intravesicular water space.

The estimated $[Ca^{2+}]_{ATPase}/[Ca^{2+}\text{-ATPase}]$ molar ratios before and after the photolysis in the experimental and control trials was subsequently further analyzed taking into full account the interactions between the multiple equilibria involved for both calcium and magnesium binding using the program of Fabiato (20). This analysis indicated, irrespective of the ranges of K_d values reported in the literature for the Ca^{2+} binding to the various components (EGTA, DM-nitrophen, and Ca^{2+}-ATPase) and the stated (see Methods) uncertainty in $[Ca^{2+}]_{residual}$, that: (a) the $[Ca^{2+}]_{ATPase}/[Ca^{2+}\text{-ATPase}]$ molar ratio before the photolysis in both the experimental and control trials was $<3:5$, (b) the $[Ca^{2+}]_{ATPase}/[Ca^{2+}\text{-ATPase}]$ molar ratio after photolysis in the experimental trials became $\sim 8:5$ while remaining $<3:5$ in the control trials, (c) the difference in the $[Ca^{2+}]_{ATPase}/[Ca^{2+}\text{-ATPase}]$ molar ratio after versus before the photolysis was greater in the experimental trials than in the control trials by a factor of 2.5–5, and (d) the unbound (or free) $[Ca^{2+}]/[Ca^{2+}]$ATPase molar ratio in the experimental trials after photolysis was $<4 \times 10^{-6}$ M. As a result of this more correct and complete analysis, it remains reasonable to conclude that the small, but experimentally significant changes in the meridional x-ray diffraction upon photolysis for the experimental trials indeed results from high-affinity calcium binding to the Ca^{2+}-ATPase, namely a transition from $Ca_{.6}E_1$ to $Ca_{1.6}E_1$, and not from low-affinity binding to other membrane components. However, it may not be correct to claim that the initial state of the enzyme was E_1 when the upper limit for the $[Ca^{2+}]_{ATPase}/[Ca^{2+}\text{-ATPase}]$ molar ratio before the photolysis may have been as high as 3:5, as compared with the estimated value of 1:100.

The difference between the electron density profiles for the isolated SR membrane before and after photolysis of the DM-nitrophen:Ca^{2+} complex in the oriented multilayer for the experimental trials, contained within $\Delta\rho_{uc}(z)$, was derived unambiguously from the changes

in the multilayer's meridional x-ray diffraction upon photolysis and is therefore similarly experimentally significant and reproducible. These changes in the SR membrane electron density profile upon photolysis for the experimental trials, contained within $\Delta\rho_{uc}(z)$, have been modeled with a step-function profile refined in real-space at ~ 13-Å resolution in order to interpret the changes with respect to the positions of the membrane's molecular components within the membrane profile. Upon photolysis, three steps of increased electron density occur at ~ 5, ~ 30, and ~ 67 Å (steps 1, 3, and 5 in Fig. 6 B) in the SR membrane profile corresponding to the region containing the polar headgroups of the inner phospholipid monolayer and Ca^{2+}-ATPase at the intravesicular membrane surface, the center of the membrane phospholipid bilayer, and the junction of the "stalk" and "headpiece" of the Ca^{2+}-ATPase protruding from the extravesicular membrane surface, respectively. Two steps of decreased electron density occur upon photolysis, namely step 2 adjacent to steps 1 and 3 of increased electron density, and step 6 adjacent to step 5 of increased electron density (refer to Fig. 6 B). The positions of these changes in the SR membrane upon photolysis have been found to be the same (to within ± 2 Å) for the several experimental trials investigated.

The small positive changes in $\Delta\rho_{uc}(z)$ can be explained on the basis of their amplitudes, by an increase in the number of electrons present in these three steps 1, 3, and 5 directly due to Ca^{2+} binding within these three distinct regions of the SR membrane profile upon its photolytic release from the DM-nitrophen. The "smallness" of the positive changes is fully consistent with the binding of one or less Ca^{2+} ions per step per enzyme molecule, averaged over the enzyme ensemble (given the atomic number of calcium, the molecular weights of the SR Ca^{2+}-ATPase and phospholipids, and the phospholipid/Ca^{2+}-ATPase ratio). The distribution and stoichiometry of calcium binding among these three distinct regions can not be quantified from this experiment since the increased electron density within these regions could also arise from conformational changes in the Ca^{2+}-ATPase profile structure, on the time scale of this time-resolved experiment (5 min), localized to these three regions. However, the small negative changes in $\Delta\rho_{uc}(z)$ for steps 2 and 6 must be due to small decreases in the electron density of the Ca^{2+}-ATPase arising from conformational changes localized to these two particular regions of its profile structure, given the time scale of this time-resolved experiment.

To determine whether changes in the SR membrane profile upon photolysis of DM-nitrophen in the experimental trials, as exhibited in $\Delta\rho_{uc}(z)$, could arise solely from Ca^{2+} binding within steps 1, 3, and 5, we attempted to model the changes in $\Delta\rho_{uc}^{exp}(z)$ with a step-function model profile that included only the positive steps from the model in Fig. 6 B (steps 1, 3, and 5). This model profile also tested whether the negative steps in the
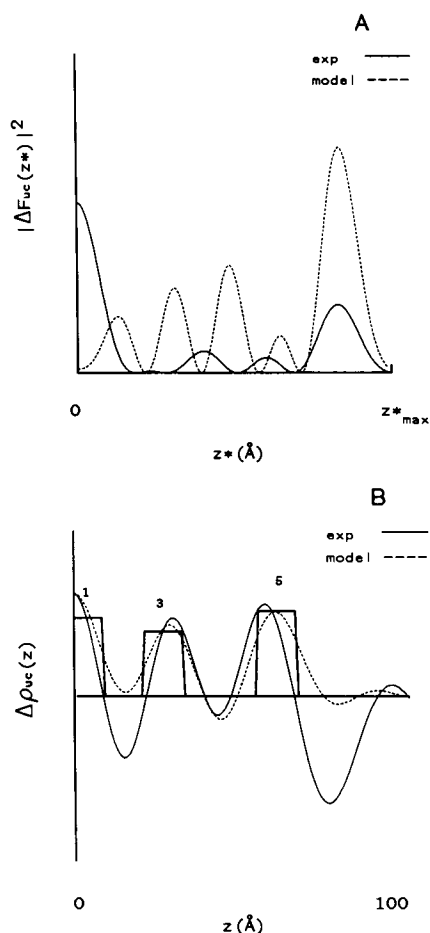
FIGURE 7   (A) The model (dotted line) unit cell structure factor modulus squared, $|\Delta F_{uc}^{mod}(z^*)|^2$, corresponding to only the positive (i.e., increased electron density) steps 1, 3, and 5 in the refined step-function model profile of Fig. 6 B (as shown in B) compared with the experimental unit cell structure factor modulus squared, $|\Delta F_{uc}^{exp}(z^*)|^2$ (solid line), for the difference electron density profile, $[\Delta\rho_{uc}^{exp}(z)]$. (B) The step-function model profile (heavy solid line) containing only the positive steps 1, 3, and 5 of the refined step-function model of Fig. 6 B for the changes in the unit cell relative electron density profile upon photolysis of the DM-nitrophen in the multilayer for the experimental trials, $[\Delta\rho_{uc}^{exp}(z)]$ (solid line), and, for comparison, this model's corresponding continuous profile, $[\Delta\rho_{uc}^{mod}(z)]$ (dotted line).

model profile of Fig. 6 B, namely steps 2 and 6, were real or simply artifacts of Fourier transform truncation. Fig. 7 shows the structure factor modulus squared, $|F_{uc}(z)|^2$ (dotted line, A), and the corresponding continuous $\Delta\rho_{uc}(z)$ (dotted line, B) for this three-step model (heavy solid line, B) versus the experimental $\Delta\rho(z)_{uc}^{exp}$ (continuous solid line, B). The three-step model profile clearly fails to fully explain the changes in $\Delta\rho_{uc}^{exp}(z)$ and firmly establishes the existence of the decreased electron density localized to steps 2 and 6 of the model profile in Fig. 6 B.

The identification of the three discrete regions of increased electron density in $\Delta\rho_{uc}(z)$ for the Ca^{2+}-ATPase as the locations of Ca^{2+} binding sites within the SR

membrane profile is strongly supported by lanthanide resonance x-ray diffraction experiments, which have located three distinct high affinity metal binding sites at the same positions in the profile of the SR membrane (reference 15; Asturias, F. J., R. Fischetti, and J. K. Blasie, manuscript submitted for publication). Other investigators have shown that lanthanide [III] ions are effective calcium analogues since they compete with Ca^{2+} for the high affinity binding sites on the Ca^{2+}-ATPase (21, 22) and they displace Ca^{2+} from specific sites on the enzyme with biphasic kinetics, similar to those observed in isotopic Ca^{2+} chase experiments and attributed to a sequential exchange mechanism (23). The recent Tb^{3+} resonance x-ray diffraction work demonstrated that the experimentally determined resonant metal atom profile represented a minimum of three discrete metal sites within the SR membrane profile located at ~2.5 Å corresponding to the intravesicular membrane surface, at ~35 Å corresponding to the center of the membrane phospholipid bilayer, and at ~63 Å corresponding to the junction of the stalk and the headpiece of the Ca^{2+}-ATPase (Asturias, F. J., R. Fischetti, J. K. Blasie, manuscript submitted for publication), whereas the previous La^{3+} resonance x-ray diffraction work (15) identified only the ~2.5- and ~63-Å sites because of its lesser capacity to displace Ca^{2+} (Asturias, F. J., R. Fischetti, and J. K. Blasie, manuscript submitted for publication).

To better understand the significance of the locations of the three discrete regions of Ca^{2+} binding and the adjacent regions of decreased electron density upon Ca^{2+} binding within the SR membrane profile, as shown schematically in Fig. 8, it is helpful to compare these results with the locations of Ca^{2+}-binding sites suggested by site-directed mutagenesis experiments (24, 25) based on a putative secondary/tertiary structure for the Ca^{2+}-ATPase predicted from its primary amino acid sequence (26, 27). The outermost site centered at ~67 Å lies outside the membrane phospholipid bilayer at the junction of the extramembraneous globular domain or headpiece and the outer end of the transmembraneous bundle of α helices or stalk of the putative structure (26). It has been suggested (26) that this site could be involved in Ca^{2+} transport but is not essential for enzyme activation. The negative region in $\Delta\rho_{uc}(z)$ arising from a decreased electron density of the Ca^{2+}-ATPase upon Ca^{2+} binding adjacent to this outermost Ca^{2+}-binding region is therefore indicative of a local conformational change occurring in the headpiece of the Ca^{2+}-ATPase. The site centered at ~30 Å is located within the transmembrane domain, consisting of a bundle of 10 α helices, near the center of the membrane phospholipid bilayer in the putative structure (26). Clarke et al. (26) have discussed the location of such a Ca^{2+}-binding site within the transmembrane helices, composed of six charged residues, and thought it to be essential for Ca^{2+} transport and enzyme activation. The innermost site at ~5 Å corresponding to the intravesicu-
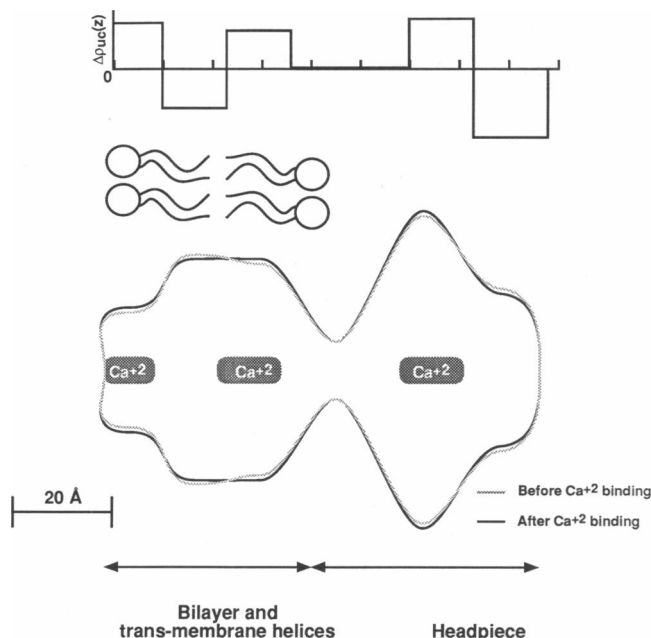
FIGURE 8 Schematic of the cylindrically averaged profile structure of the SR Ca^{2+}-ATPase within the membrane phospholipid bilayer with the difference step-function model $[\Delta\rho_{uc}^{exp}(z)]$ shown at the top. The three different positions of high-affinity Ca^{2+} binding within the profile structure of the *unphosphorylated* enzyme seen in this study, corroborated by independent results from lanthanide resonance x-ray diffraction experiments, are indicated.

lar membrane surface could be either a protein or a phospholipid headgroup binding site. The negative region in $\Delta\rho_{uc}(z)$ arising from a decreased electron density of the Ca^{2+}-ATPase upon Ca^{2+} binding adjacent to these two sites at $\sim$5 and $\sim$30 Å would then correspond to a conformational change within the transmembrane α-helical bundle (e.g., a slight expansion of the area per helix in the membrane plane) localized to this region between these two sites.

CONCLUSION

Upon flash-photolysis of the caged-calcium molecule, DM-nitrophen, in an oriented membrane multilayer, the electron density profile of the SR membrane exhibits small, but significant changes arising from high-affinity calcium binding to the Ca^{2+}-ATPase. The origin of these changes has been attributed to three distinct regions of Ca^{2+} binding to the unphosphorylated enzyme, centered at $\sim$5, $\sim$30, and $\sim$67 Å in the membrane profile and corresponding to the intravesicular surface, the "transbilayer" domain near the center of the phospholipid bilayer, and the junction of the stalk/headpiece domain of the enzyme, respectively. In addition to these three distinct Ca^{2+}-binding regions of increased electron density in the membrane profile, two regions of decreased electron density also occur upon calcium binding. These two regions lie between the $\sim$5- and the $\sim$30-Å Ca^{2+}-bind-

ing sites and adjacent the $\sim$67-Å site, respectively, and indicate that conformational changes occur within the Ca^{2+}-ATPase localized to these two regions of the membrane profile as a result of the Ca^{2+}-binding reaction. The Ca^{2+}-binding locations within the membrane profile identified here correspond to metal binding sites determined independently by lanthanide resonance x-ray diffraction studies (reference 15; Asturias, F. J., R. Fischetti, and J. K. Blasie, manuscript submitted for publication) employing the lanthanide as a calcium analogue and agree with those predicted by a putative structure for the Ca^{2+}-ATPase along with related site-directed mutagenesis studies (24–27).

REFERENCES

1. deMeis, L., and A. L. Vianna. 1979. Energy interconversion by the Ca^{2+}-dependent ATPase of the sarcoplasmic reticulum. *Annu. Rev. Biochem.* 48:275–292.

2. Inesi, G. 1987. Sequential mechanism of calcium binding and translocation in the sarcoplasmic reticulum adenosine triphosphatase. *J. Biol. Chem.* 262:16338–16342.

3. Dupont, Y. 1979. Fluorescent studies of the sarcoplasmic reticulum calcium pump. *Biochem. Biophys. Res. Commun.* 71:544–550.

4. DeLong, L. J., C. M. Phillips, J. H. Kaplan, A. Scarpa, and J. K. Blasie. 1990. A new method for monitoring the kinetics of calcium binding to the sarcoplasmic reticulum Ca^{2+}-ATPase employing the flash photolysis of caged-calcium. *J. Biochem. Biophys. Methods* 21:333–339.

5. Blasie, J. K., L. G. Herbette, D. Pascolini, D. H. Pierce, and A. Scarpa. 1985. Time resolved x-ray diffraction studies of the sarcoplasmic reticulum membrane during active transport. *Biophys. J.* 48:9–18.

6. Pascolini, D., L. G. Herbette, V. Skita, F. Asturias, A. Scarpa, and J. K. Blasie. 1988. Changes in the sarcoplasmic reticulum membrane profile induced by enzyme phosphorylation to $E_1 \sim P$ at 16 Å resolution via time-resolved x-ray diffraction. *Biophys. J.* 54:679–688.

7. Asturias, F. J., and J. K. Blasie. 1989. Effect of Mg^{2+} concentration on Ca^{2+} uptake kinetics and structure of the sarcoplasmic reticulum membrane. *Biophys. J.* 55:739–753.

8. Herbette, L., A. Marquardt, A. Scarpa, and J. K. Blasie. 1977. A direct analysis of lamellar x-ray diffraction from hydrated oriented multilayers of fully functional sarcoplasmic reticulum. *Biophys. J.* 20:245–272.

9. Herbette, L., P. DeFoor, S. Fleischer, D. Pascolini, A. Scarpa, and J. K. Blasie. 1985. The separate profile structures of the calcium pump protein and the phospholipid bilayer within isolated sarcoplasmic reticulum membranes determined by x-ray and neutron diffraction. *Biochim. Biophys. Acta.* 817:103–122.

10. Ellis-Davies, G. C. R., and J. H. Kaplan. 1988. Photolabile chelators for the rapid photorelease of divalent cations. *Proc. Natl. Acad. Sci. USA.* 85:6571–6575.

11. Pierce, D. H., A. Scarpa, M. R. Topp, and J. K. Blasie. 1983. Kinetics of calcium uptake by isolated sarcoplasmic reticulum vesicles using flash photolysis of caged adenosine 5'-triphosphate. *Biochemistry.* 22:5254–5261.

12. Dipolo, R., J. Requena, F. J. Brinley, Jr., L. J. Mullins, A. Scarpa, T. Tiffert. 1976. Ionized calcium concentrations in squid axons. *J. Gen. Physiol.* 67:433–467.

13. Fabiato, A. 1981. Myoplasmic free calcium concentration reached during the twitch of an intact isolated cardiac cell and during calcium-induced release of calcium from the sarcoplasmic reticulum of a skinned cardiac cell from the adult rat or rabbit ventricle. *J. Gen. Physiol.* 78:457–497.

14. Pascolini, D., and J. K. Blasie. 1988. Moderate resolution profile structure of the sarcoplasmic reticulum membrane under "low" temperature conditions for the transient trapping of the $E_1 \sim$ P. *Biophys. J.* 54:669–678.

15. Asturias, F. J., and J. K. Blasie. 1991. Location of high-affinity metal binding sites in the profile structure of the Ca^{2+}-ATPase in the sarcoplasmic reticulum by resonance x-ray diffraction. *Biophys. J.* 59:488–502.

16. Kaplan, J. H. 1990. Photochemical manipulation of divalent cation levels. *Annu. Rev. Physiol.* 52:897–914.

17. Kaplan, J. H. 1986. Caged ATP as a tool in active transport research. *In* Optical Methods in Cell Physiology. P. DeWeer and B. M. Salzberg, editors. Wiley-Interscience, New York. 385–396.

18. Warren, B. E. 1969. X-ray Diffraction. Addison-Wesley Publishing Co., Reading, MA. 381 pp.

19. Schwartz, S., J. E. Cain, E. A. Dratz, and J. K. Blasie. 1975. An analysis of lamellar x-ray diffraction from disordered membrane multilayers with application to data from retinal rod outer segments. *Biophys. J.* 15:1201–1233.

20. Fabiato, A. 1988. Computer programs for calculating total from specified free or free from specified total ionic concentrations in aqueous solutions containing multiple metals and ligands. *Methods Enzymol.* 157:378–417.

21. Highsmith, S., and M. Head. 1983. Tb^{3+} binding to Ca^{2+} and Mg^{2+} binding sites on the sarcoplasmic reticulum ATPase. *J. Biol. Chem.* 258:6858–6862.

22. Scott, T. 1983. Luminescence studies of Tb^{3+} bound to the high affinity sites of the Ca^{2+}-ATPase of the sarcoplasmic reticulum. *J. Biol. Chem.* 259:4035–4037.

23. Squier, T. C., D. J. Bigelow, F. J. Fernandez-Belda, L. deMeis, and G. Inesi. 1990. Calcium and lanthanide binding in the sarcoplasmic reticulum ATPase. *J. Biol. Chem.* 265:13713–13720.

24. MacLennan, D. H., C. J. Brandl, B. Korczak, N. M. Green. 1985. Amino-acid sequence of a Ca^{2+} + Mg^{2+}-dependent ATPase from rabbit muscle sarcoplasmic reticulum, deduced from its complementary DNA sequence. *Nature (Lond.).* 316:696–700.

25. Clarke, D., K. Maruyama, T. Loo, E. Leberer, G. Insei, and D. MacLennan. 1989. Functional consequences of glutamate, aspartate, glutamine, and asparagine mutations in the stalk sector of the Ca^{2+} ATPase of sarcoplasmic reticulum. *J. Biol. Chem.* 264:11246–11251.

26. Clarke, D., T. Loo, G. Inesi, and D. MacLennan. 1989. Location of high affinity Ca^{2+}-binding sites within the predicted transmembrane domain of the sarcoplasmic reticulum Ca^{2+} ATPase. *Nature (Lond.).* 339:476–478.

27. Brandl, C. J., N. M. Green, B. Korczak, and D. H. MacLennan. 1986. Two Ca^{2+} ATPase genes: homologies and mechanistic implications of deduced amino acid sequences. *Cell.* 44:597–607.